2015 IEEE International Conference on Advanced Intelligent Mechatronics (AIM)
July 7-11, 2015. Busan, Korea

Optimization Design of the Inner Radius of the Sealing Surface of Slipper*

Qian-nan Wang, Bing Xu, and Jun-hui Zhang

Abstract— **A dynamic lubrication model is built based on the lubrication theory of the oil film for optimization design of the inner radius of the sealing surface of slipper, considering the macro and micro motion of the slipper. Reasonable design criterion is presented, adopting the oil film characteristics, dynamic stiffness and minimum power loss as the optimum conditions. Furthermore, the experiments of the pump efficiency are done under the given working conditions. The results suggest that the pump with optimized slippers obtains the better oil film characteristics and efficiency, and the proposed design criterion could be applied as references for slipper/swash-plate pair design.**

Nomenclature

R_c	Pitch radius of the piston
β	Swash plate angle
r_p	Piston radius
r_b	Piston ball radius
l_{d1},d_{d1}	Structure parameters of orifice of piston
l_{d2},d_{d2}	Structure parameters of orifice of slipper
r	Distance between the point at the bottom and the center of slipper
r_1	Inner radius of sealing surface
r_2	Outer radius of sealing surface
ρ	Equivalent radius of oval trajectory of slipper
r_M	Distance between the point at the bottom and the center of the oval trajectory
α	Slipper tilting angle
φ	Angular position of the slipper from BDC
θ	Angle between radius vector and y axis
δ	Angle between v_s and the direction radially outwards
l_{sg}	Distance between the slipper gravity center and the spherical center
l_s	Distance between the bottom of the slipper and the spherical center
ω	Angular velocity of the shaft
ω_s	Angular velocity of the slipper
ω_z	Slipper spin angular velocity
a_z	Slipper spin angular acceleration
v_{sr}	Couette flow velocity in the radial direction
$v_{s\theta}$	Couette flow velocity in the circumferential direction
v_s	Couette flow velocity
F_s	Spring force
$F_{\omega s}$	Centrifugal force of slipper
F_p	Inhaling force
F_f	Friction force
F_a	Inertial force of piston/slipper assembly
F_{sa}	Lifting force
F_N	Clamping force
J	Dynamic stiffness
$\tau_{s\theta}$	Shear stress in the circumferential direction
τ_{sr}	Shear stress in the radial direction
v_r	Flow velocity of the control volume
h_1,h_2,h_3	Gap height of the three points on outer edge at an interval of 120 degrees
z	Oil film thickness
k	Stiffness of cylinder spring
x	Pre-compressing quantity of cylinder spring
p_d	Operating pressure
p_s	Suction pressure
p_r	Pressure in the slipper pocket
p	Pressure under the sealing surface
p_d	Case drain pressure
P_F	Friction power loss of one slipper
P_L	Leakage power loss of one slipper
P_{tF}	Total friction power loss of one slipper
P_{tL}	Total leakage power loss of one slipper
P_t	Total power loss of one slipper
μ	Dynamic viscosity
m_{ps}	Mass of piston/slipper assembly
J_z	Moment of inertia of slipper
f	Friction coefficient under full-film lubrication

*Research supported by the National Basic Research Program of China (973 Program) (No. 2014CB046403), the National Natural Science Foundation of China (No.51075360), the National Key Technology R&D Program of the Twelfth Five-year Plan of China (2013BAF07B01).

Qian-nan Wang is with the State Key Laboratory of Fluid Power Transmission and Control, Zhejiang University, *Hangzhou 310027 China* (e-mail: qiannanw@zju.edu.cn).

Bing Xu is with the State Key Laboratory of Fluid Power Transmission and Control, Zhejiang University, *Hangzhou 310027 China* (phone: +86-0571-87951387; fax: +86-0571-87952507; e-mail: bxu@zju.edu.cn).

Jun-hui Zhang is with the State Key Laboratory of Fluid Power Transmission and Control, Zhejiang University, *Hangzhou 310027 China* (e-mail: benzjh@zju.edu.cn).

I. Introduction

Servo-hydrostatic actuators are widely used for flight control in aerospace nowadays, which are supplied at a constant pressure from centralized hydraulic pumps driven by engines. Unlike industrial pump, the operating condition of the pump used in aerospace is much more adverse. As we know, the slipper is connected with the piston via a spherical joint. The slipper is not parallel with the swash plate under the action of external forces and moments. The oil film between slipper and swash plate is crucial from the viewpoint of the efficiency and reliability of the pump, so it is necessary to clarify the design criterion of the bearing and sealing pairs.

Traditionally, slippers are designed to operate partially hydrostatically. The forces and moments generated by hydrostatic pressure are nearly in balance with the external loads, only leaving a small residual clamping load to be carried by the hydrodynamic pressure and squeezing pressure. The inner radius r_1 of the sealing surface shown in Fig.1 is the key structural parameter to determine the hydrostatic load and the ratio between the hydrostatic and hydrodynamic loads. But there is rare research about the inner radius design of the sealing surface of slipper in the published papers for industrial pumps, let alone pumps used in aerospace. T. Kazama and A. Yamaguchi[1] treated the circular hydrostatic thrust bearings as the sealing parts in hydraulic equipment and discussed the reasonable design criterion based on the optimum conditions, i.e. the minimum power loss, the minimum size and the maximum stiffness. N. Iboshi and A. Yamaguchi[2-4] also expanded this design criterion into the sealing surface

optimization design of slipper for swash plate type axial piston pumps and motors. However, all those researches are based on the assumption that the surfaces of the friction pairs are parallel. Slippers are tilted under the action of titling moments due to the centrifugal force and friction forces. The wedge-shaped oil film generates squeezing and hydrodynamic pressures along with the slipper's motion. However, partial abrasion occurs due to solid-to-solid contact at the position where the oil film is too thin if severe tilt of the slipper happens. Therefore, the inner radius design of the sealing surface of slipper should take the dynamic working conditions especially during the transition between high delivery pressure and low suction pressure into consideration.

For the last several decades, researchers have done a lot of theoretical and experimental researches about the carrying mechanism of the oil film between the slipper/swash-plate pairs. Hooke[5-9] concluded the major forces for the slipper tilt were from the friction forces of the spherical joint and piston-cylinder pair, and tilting was necessary to produce the desired hydrodynamic lift. Koç[10-12] focused their work on studying the impact of the slipper geometry on the characteristics of the oil film. Fazil[13] analyzed leakage, frictional power loss in a hydrostatic bearing system considering the size of bearing pocket and the orifice dimension. Harris[14] created a mathematical dynamic model for slipper which was able to handle the effect of the possible contact with the swash plate. Wieczoreck and Ivantysynova[15-17] developed a fluid-structure-thermal coupled simulation model of axial piston pump, which is verified by the experimental results of test rigs for oil film characteristics measurement. Although the above authors have analyzed the lubrication and carrying mechanism of the slipper in detail, they did not presented a complete and accurate design method about the sealing surface of slipper, especially the inner radius.

In this paper, the attention is focused on giving a reasonable design criterion for the optimization design of the sealing surface of slipper, adopting the dynamic oil film characteristics, dynamic stiffness, minimum power loss as the optimum conditions. A numerical simulation model is developed based on the lubrication theory of the oil film, considering macro/micro motion of slipper. With the simulation model, the relationships between the inner radius of the sealing surface and oil film thickness, pressure distribution, dynamic stiffness and power loss are discussed in detail. The results show that it is an effective method for designing compact, reliable, and high-efficiency hydraulic axial piston pumps.

II. Procedure for Paper Submission

The forces and motion characteristics of slipper are most complicated in axial piston pump. Fig.1 shows the force condition, the relevant kinematic parameters and the key dimensions of the piston/slipper assembly. In order to simplify the calculation of slipper motion characteristics and external forces, a Cartesian coordinate system fixed with the center of slipper is selected. The slipper rotates about the main shaft and slides on the swash plate. Moreover, the slipper rotates about its own axis due to the friction moment of spherical joint. So the slipper moves with a tangential velocity "v_s", and spins with an angular velocity "ω_z".

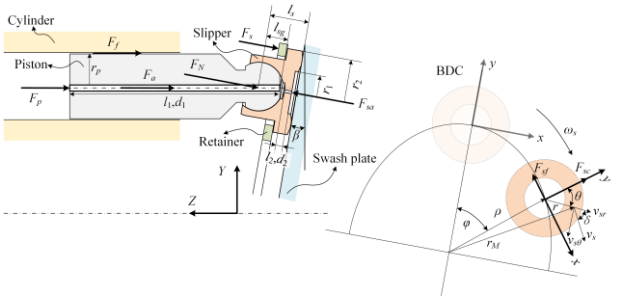

Figure 1. Diagram of slipper/piston assembly

2.1. Kinematics analysis

The template is used to format your paper and style the text. All margins, column widths, line spaces, and text fonts are prescribed; please do not alter them. You may note peculiarities. For example, the head margin in this template measures proportionately more than is customary. This measurement and others are deliberate, using specifications that anticipate your paper as one part of the entire proceedings, and not as an independent document. Please do not revise any of the current designations.

$$v_s = r_M \omega_s$$

$$v_{sr} = v_s \cos\delta; v_{s\theta} = \begin{cases} v_s \sin\delta & -\frac{\pi}{2} \le \theta \le \frac{\pi}{2} \\ -v_s \sin\delta & \frac{\pi}{2} \le \theta \le \frac{3\pi}{2} \end{cases} \quad (1)$$

So the spin angular acceleration can be determined by (2) and the spin angular velocity can be obtained by integrating the spin angular acceleration.

$$J_z a_z = f F_N r_q \cos\beta - \int_{\theta=0}^{\theta=2\pi} \int_{r=r_1}^{r=r_2} \tau_{s\theta} r^2 d\theta dr \quad (2)$$

The slipper maintains in a dynamic balance state and the titling angle and azimuth angle vary with the oscillating external clamping force and moments as shown in Fig.2. Neglecting the surface deformation of slipper, the micro oscillating motion of slipper can be calculated by the three points on the outer edge at an interval of 120 degrees which can be described by (3). The influence of the surface deformation will be taken into consideration in the simulation model for the next step.

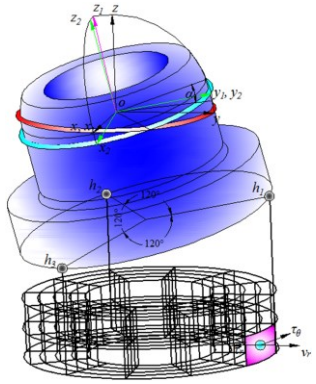

Figure 2. Sketch of the tilted slipper

$$\frac{\partial h(r,\theta)}{\partial t}=\sqrt{\frac{1}{3}}\frac{\left(h_2^{'}-h_3^{'}\right)r\sin\theta}{r_2}+\frac{\left(2h_1^{'}-h_2^{'}-h_3^{'}\right)r\cos\theta}{3r_2}+\frac{h_1^{'}+h_2^{'}+h_3^{'}}{3} \tag{3}$$

The oil film thickness at an arbitrary point (r, θ, z) on the slipper sealing surface can be obtained using (3) during the simulation. So the maximum or minimum oil film thickness of every simulation step is easily found and the tilting angle of the slipper is obtained by the following equation:

$$a_t=\arcsin\left(\frac{h_{\max}-h_{\min}}{2r_2}\right) \tag{4}$$

2.2. Forces analysis

The oil film is regarded as laminar flow with micrometer-scale gap height. The Reynolds equation for oil film between slipper and swash plate can be obtained by the two dimensional Navier-Stokes equation and the continuity equation which can be expressed by:

$$\frac{1}{r}\frac{\partial}{\partial r}\left(r\frac{h^3}{\mu}\frac{\partial p}{\partial r}\right)+\frac{1}{r^2}\frac{\partial}{\partial\theta}\left(\frac{h^3}{\mu}\frac{\partial p}{\partial\theta}\right)=6v_{sr}\frac{\partial h}{\partial r}+6\left(\frac{v_{s\theta}}{r}+\omega_z\right)\frac{\partial h}{\partial\theta}+12\frac{\partial h}{\partial t} \tag{5}$$

Pressure distribution is obtained by solving the Reynolds Equation using the finite volume method. The pressure boundary is determined by the pressure in the slipper pocket and the case drain pressure. The fluid flows into slipper pocket from piston chamber via orifices and flows out of slipper pocket through a variable annular narrow clearance. So the pressure in the slipper pocket is determined by the following equation:

$$\frac{\pi\left(l_{d2}d_{d1}^4+l_{d1}d_{d2}^4\right)}{128\mu l_{d1}l_{d2}}\left(p_s-p_r\right)=\int_{\theta=0}^{\theta=2\pi}\int_{z=0}^{z=h}v_r r_2 d\theta dz \tag{6}$$

The clamping force acted on the slipper is expressed as:

$$F_N=\frac{F_p+F_a+F_f+F_s}{\cos\beta} \tag{7}$$

The force and moments generated by the oil film are balanced with the oscillating external clamping force and moments. In order to the determinate of the pressure force acted on the piston, the instantaneous cylinder pressure is calculated by the hydraulic simulation model of axial piston pump[18]. The normal clamping force is in equilibrium with the lifting force generated by oil film which can be determined by the following equation:

$$F_{sa}=\pi r_1^2 p_r+\int_{\theta=0}^{\theta=2\pi}\int_{r=r_1}^{r=r_2}prdrd\theta \tag{8}$$

The slipper reaches a dynamic balance state when the titling moment is in equilibrium with the anti-overturning moment generated by oil film under the slipper. The two equilibrium equations are shown as follows:

$$F_{\omega s}l_{sg}\cos\beta-fF_N r_b\sin\beta\cos\varphi=\int_{\theta=0}^{\theta=2\pi}\int_{r=r_1}^{r=r_2}pr^2\cos\theta drd\theta \tag{9}$$

$$\int_{\theta=0}^{\theta=2\pi}\int_{r=r_1}^{r=r_2}\tau_t rl_s drd\theta-fF_N r_b\sin\beta\sin\varphi=\int_{\theta=0}^{\theta=2\pi}\int_{r=r_1}^{r=r_2}pr^2\sin\theta drd\theta \tag{10}$$

The friction force between slipper and swash plate is given by integrating the shear stress τ_t over sealing surface. The shear stress can be obtained from the following equation:

$$\tau_t=\left(\frac{\partial p}{\partial r}\frac{h}{2}+\mu\frac{v_{sr}}{h}\right)\sin\theta+\left(\frac{\partial p}{r\partial\theta}\frac{h}{2}+\mu\frac{v_{sr}+r\omega_z}{h}\right)\cos\theta \tag{11}$$

2.3. Dynamic Stiffness Analysis

As mentioned above, slippers are designed to operate partially hydrostatically. If the external clamping force applied on the slipper increases, the oil film thickness decreases, and then the leakage through the variable annular narrow clearance decreases, so the pressure in the slipper pocket increases and the carrying capacity of the oil film under the slipper increases and vice versa. Therefore, the oil film works like a spring. A large dynamic stiffness can improve the stability and load capacity of the oil film and it can be evaluated as:

$$J=-\frac{dF_{sa}}{dh} \tag{12}$$

2.4. Power Loss Analysis

The power loss of the slipper/swash-plate pair is composed of friction power loss and leakage power loss. Friction power loss of a single slipper/swash-plate pair is determined based on the shear stress on the sliding surface in every control volume (r, θ).

$$\frac{\pi\left(l_{d2}d_{d1}^4+l_{d1}d_{d2}^4\right)}{128\mu l_{d1}l_{d2}}\left(p_s-p_r\right)=\int_{\theta=0}^{\theta=2\pi}\int_{z=0}^{z=h}v_r r_2 d\theta dz \tag{13}$$

Leakage power loss is obtained by multiplying pressure drop and leakage flow, while the leakage flow is obtained by integrating the velocity distribution in radial direction over the gap height.

$$P_L=\int_{\theta=0}^{\theta=2\pi}\int_{r=r_1}^{r=r_2}\Delta p\left[\frac{1}{2\mu}\frac{\partial p}{\partial r}\left(z^2-zh\right)+v_{sr}\frac{z}{h}\right]rdzd\theta \tag{14}$$

Based on the above analysis, a simulation model is built and the nonlinear equations in the simulation model are solved by the successful adoption of Newton iterative method via the squeezing effect as a bridge combining the external force/moments with the oil film characteristics. The simulation procedure is shown in Fig.3. The simulation model can be verified by the test rig for the oil film measurement which has been designed and is being manufactured. However, a numerical simulation model of the piston/cylinder pair has been already developed based on the same lubrication theory

of the oil film and a model pump for pressure distribution measurement of oil film between piston and cylinder bore has been built[19]. The comparison of simulation and experimental results of pressure distribution showed that the simulation model of the piston/cylinder pair has a satisfying accuracy, which verifies the correctness of the lubrication model of the slipper indirectly.

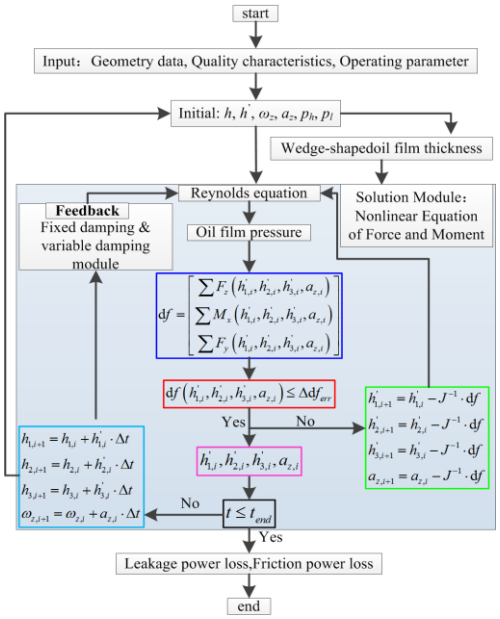

Figure 3. Simulation Procedure

III. Simulation Results and Discussion

The main geometrical parameters and operating conditions of the simulation are shown in table I and table II respectively.

TABLE I. Geometrical Parameters of the Simulation

Geometrical Parameters	*Value*	*Unit*
R_c	27.5	mm
β	18	deg
r_p	7.1	mm
r_b	6	mm
r_2	7.95	mm
l_{d1}, d_{d1}	1.5, 0.8	mm
l_{d2}, d_{d2}	53.0, 2.3	mm
k	68.2	N/m
x	5.5	mm

TABLE II. Operating Conditions of the Simulation

Operating conditions	*Value*	*Unit*
μ	0.01089	Pa·s
p_s	5	bar
p_d	300	bar
$n_{o\,max}$	4000	min^{-1}

3.1. Analysis of oil film characteristics

The pressure distribution and film thickness at a moment during the delivery stroke are shown in Fig. 4. The pressure distribution is asymmetric along the slipper angular position. The local pressure on the right-half sealing land is bigger than the pressure in the slipper pocket, since the pressure ratio is greater than 1 as shown in Fig.4a. This is because the hydrodynamic pressure generates when the tilting slipper slides on the swash plate. The squeezing pressure generates because the oil film thickness decreases when the slipper is pushed towards the swash plate by the external clamping load. Since hydrodynamic and squeezing effects are in inverse correlation with the film thickness, the pressure peak occurs about where the film thickness is minimum as shown in Fig.4b. This automatically implies that the lifting force center of the oil film for the tilted slipper locates at the side where the oil film thickness is small, so anti-overturning moment generate. These moments tend to restore the slipper to zero tilt position.

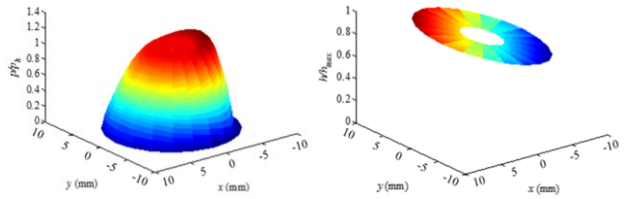

(a) (b)

Figure 4. Pressure distribution and thickness distribution

The slipper is in a dynamic balance state titling about the x and y axis. The minimum oil film thickness due to tilt should be larger than the surface roughness in order to realize complete fluid lubrication for the slipper. Therefore, it is rather important to improve the carrying ability of the oil film. As the inner radius of the sealing surface is one of the crucial parameters in the slipper design, it is worthy of investigating the performance of the slipper with different inner radii taking the pressure distribution, oil film thickness, tilting angle into consideration respectively.

3.2. Forces analysis

3.2.1 Case 1: The inner radius of sealing surface is too small or too large

When the carrying ability of the oil film is insufficient, the simulation model will stop because the force and moment equilibrium equations cannot be solved. Fig.5 depicts the oil film thickness variation with the angular position of piston when the inner radius of sealing surface is 1.0mm or 6.5mm. Both simulations failed during the transition from the delivery stroke to the suction stroke.

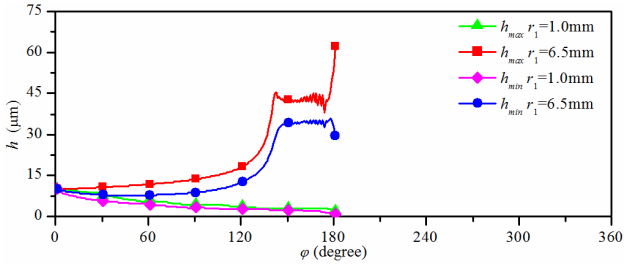

Figure 5. Oil film thickness

As mentioned in section 3.1, the hydrodynamic and squeezing pressures generate the anti-overturning moments, and they also participate in balancing the external clamping force. As for the 6.5mm inner radius of sealing surface, the hydrostatic force of the oil film in the slipper pocket is closely equal to F_p which is the main component of the external clamping force. In order to guarantee the necessary part of hydrodynamic and squeezing pressures, the leakage of slipper/swash-plate pair should be large to reduce the pressure in the slipper pocket. Therefore, the oil film thickness is quite large as shown in Fig.5. The minimum oil film thickness is even larger than 40 μm when the slipper moves to the top dead center (TDC). When the suction stroke begins, the time rate of change of the oil film thickness increases sharply due to the low load pressure. The large leakage requires a more large oil film thickness, so the slipper divorces from the swash plate and the piston pump cannot operate properly.

As for the 1.0mm inner radius of sealing surface, the oil film thickness should be small in order to improve the hydrostatic pressure, the hydrodynamic and squeezing pressures. Because the small oil film thickness can reduce the leakage which will increase the pressure in slipper pocket. As the hydrodynamic and squeezing effects are in inverse correlation with oil film thickness, the oil film thickness and tilting angle shown in Fig.6 under the slipper with 1.0mm inner radius of sealing surface is quite smaller than those of the slipper with 6.5mm inner radius of sealing surface. However the hydrostatic lifting force can only balance small part of the external clamping force for the slipper with small inner radius, leaving a large residual force which should be balanced by the hydrodynamic and the squeezing forces. The slipper requires a larger tilting angle. However, the tilting angle cannot be large when the oil film is thin, because the minimum oil film thickness will be too thin, resulting solid-to-solid contact. Then, severe partial abrasion takes place along with the spin about the slipper's central axis. When the suction stroke begins, the contradiction between the thin oil film and large tilting angle becomes more serious, and the force and moment equilibrium cannot be solved.

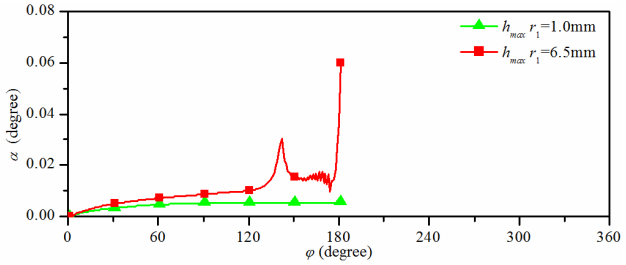

Figure 6. Maximum tilting angle

Therefore characteristics of the slipper with an inner radius of sealing surface in a range of 3.5mm to 6.0mm are studied in detail in rest of the paper. The optimal reference range of the inner radius of sealing surface is given according to several performance evaluation criterion, such as the oil film characteristics (oil film thickness, tilting angle), stiffness and total power loss.

3.2.2 Case 2: A range of 3.5mm to 6.0mm inner radii of sealing surface

The following figures show the pressure distribution of the oil film under different inner radii when the slipper locates at the delivery stroke, at an interval of 120 degrees from the bottom dead center. The growth step of the inner radius is 0.1mm in simulation, but only six simulation results are selected considering article's length and the figure's clarity.

The peak pressure of the oil film decreases along with the increasing of the inner radius, and the shape of the pressure distribution along the radius changes slowly from convex to concave as it is shown in Fig.7. This is because the hydrodynamic and squeezing pressures take more of the carrying responsibility when the inner radius is small, while the hydrostatic pressure in the slipper pocket balances with most part of the external clamping load when the inner radius is large.

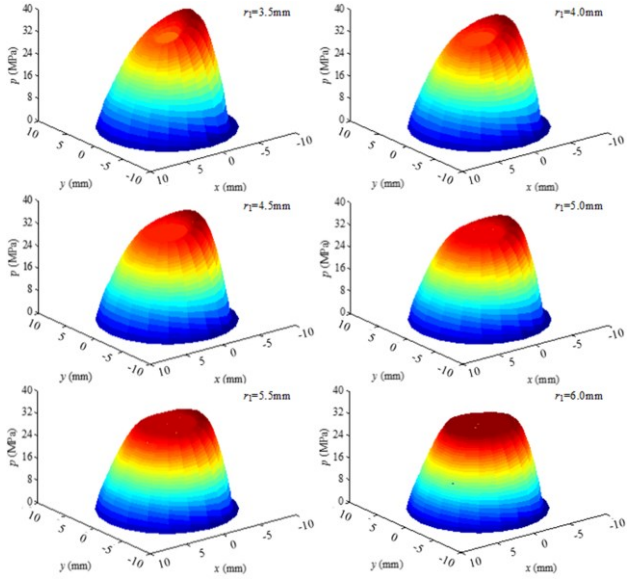

Figure 7. Pressure distribution

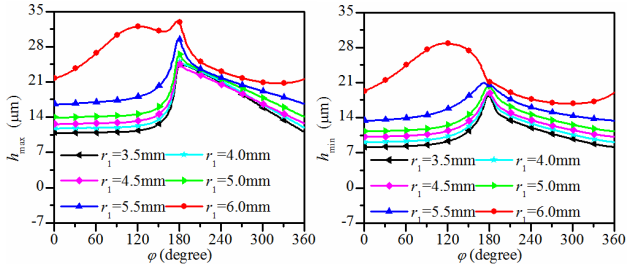

Figure 8. Minimum oil film thickness

The variations of maximum and minimum oil film thickness are shown in Fig.8. The smaller inner radius requires a higher pressure in the slipper pocket, and the thinner oil film is good to increase the pressure in the slipper pocket, which improves the hydrostatic carrying ability of the oil film. Therefore, both the maximum and minimum oil film thicknesses increase along with the increase of the inner radius as shown in Fig.8. The oil film thickness during the delivery stroke is thinner than that during the suction stroke when the inner radius is smaller than 5.5mm. However, the fact for slipper with a 6.0mm inner radius is different. This is because the inner radius is close to the piston radius, and the force equilibrium requires that the pressure in the slipper pocket

should be smaller enough to leave a small residual clamping load to be carried by the hydrodynamic and squeezing pressure. Therefore, the oil film thickness should be large enough to generate large leakage during the high-pressure delivery stroke, which helps to realize a lager pressure drop via the orifice.

As it can be seen from Fig.9, the maximum tilting angle does not exceed 0.02 degree. The slipper tilting angle is much bigger during the suction stroke than that during the delivery stroke. In other words, the slipper runs in a much more tilted position during the suction stroke. When the inner radius is larger than 5.5mm, the variation of the tilting angle is nearly the same. This is because the hydrodynamic and squeezing effects take quite small part in the force balance.

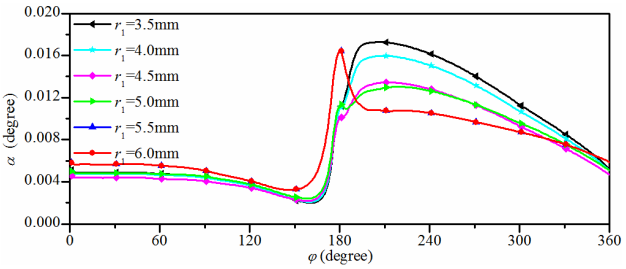

Figure 9. Maximum tilting angle

3.3. Dynamic stiffness

As mentioned above, the dynamic stiffness is crucial for the stability and load capacity of oil film. In order to guarantee the oil film has sufficient load carrying ability in a wide working parameters range, the oil film thickness should vary a little when the external clamping force changes especially during the transition regions.

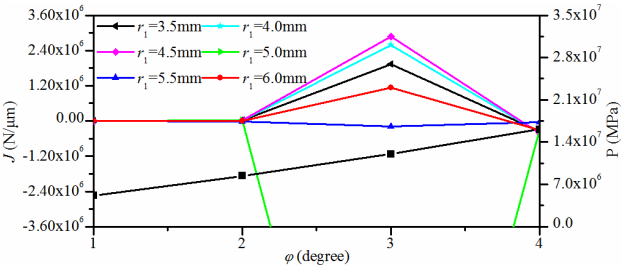

(a)

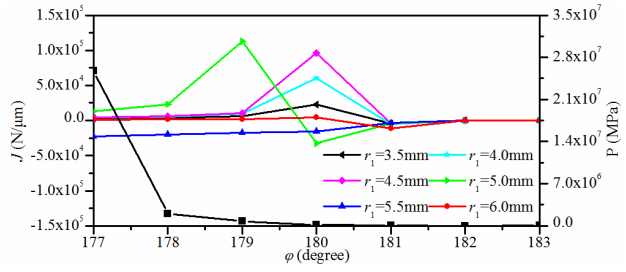

(b)

Figure 10. Dynamic stiffness of the oil film

The effect of the inner radius on the dynamic stiffness of the slipper is shown in Fig.10. The external clamping force changes sharply at TDC. Correspondingly, the oil film thickness and tilting angle vary sharply and the oil film thickness is the smallest at TDC. The oil film may be destroyed if the stability of the slipper is broken, so the dynamic stiffness during this region is critical important.

Fig.10a shows the dynamic stiffness at BDC. The pressure in piston chamber increases sharply. The dynamic stiffness of the oil film increases along with the increase of inner radius. However, the value of the dynamic stiffness becomes negative when the inner radius is bigger than 5.5mm. Similarly, Fig.10b shows the dynamic stiffness at TDC. The pressure in piston chamber decreases sharply. The dynamic stiffness of the oil film also increases along with the increase of inner radius. Although the peak value of the dynamic stiffness is largest when the inner radius is 5.5mm, part of the value is negative. So the dynamic stiffness is the best when the inner radius of the slipper is larger than 5.0mm and smaller than 5.5mm. Moreover, the dynamic stiffness of the oil film at BDC is much larger than that at TDC, which means the slipper moves more steadily at BDC. It is in coincidence with the dynamic characteristics of the oil film as shown in Fig.7~8.

3.4. Analysis of power loss

Efficiency is one of the most important characteristics for the pump. Leakage and friction power loss of the slipper/swash-plate pair are two crucial components of energy dissipation. According to the principle of conservation of energy, the power loss caused by leakage and friction leads to the temperature increase of the oil film. So it is helpful to improve the carry capacity by decreasing the power loss. Therefore the power loss is taken into consideration to help find the optimal inner radius of sealing surface. It is assumed that all the slippers in the pump have the same dynamic characteristics and the power loss in one cycle has a fixed phase difference between two adjacent slippers. The sum of the leakage power loss and the sum of the friction power loss can be obtained through the simulation as shown in Fig.11 and Fig.12 respectively.

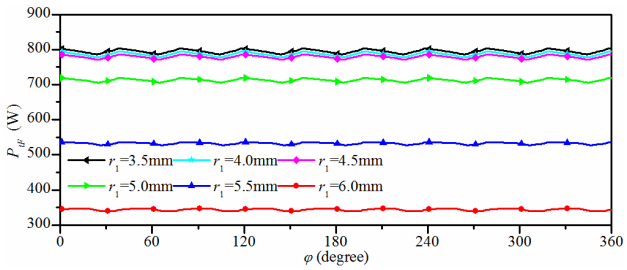

Figure 11. Total torque loss

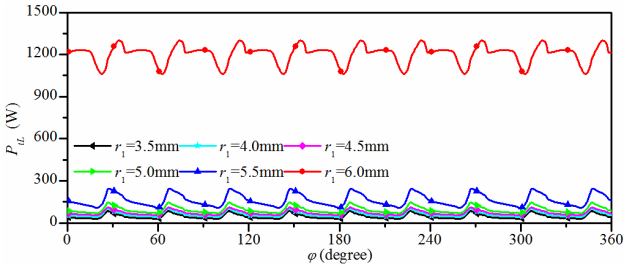

Figure 12. Total leakage loss

The friction power loss decreases with the increase of the inner radius of the sealing surface, which is because the velocity gradient of the oil film decreases with the increase of oil film thickness. The leakage power loss increases with the

increase of the inner radius, which is because the leakage increases with the increase of oil film thickness. Therefore, there exists a minimum total power loss which is the sum of the leakage power loss and the friction power loss.

The relationship between the total power loss and the inner radius of the sealing surface is shown in Fig.13. The total power loss decreases as the inner radius of the sealing surface increases. When the inner radius is bigger than 5.3mm, the power loss increases rapidly with the increase of the inner radius. As we can see from Fig.11~12, the increase magnitude of the leakage loss is bigger than decrease magnitude of the torque loss when the inner radius of the sealing surface is bigger than 5.3mm. So the total power loss increases sharply when the inner radius increases further. It is obvious that the total power loss is minimum when the inner radius of sealing surface is 5.3mm. So it is proposed that 5.3mm is the recommended value for the inner radius of the sealing surface.

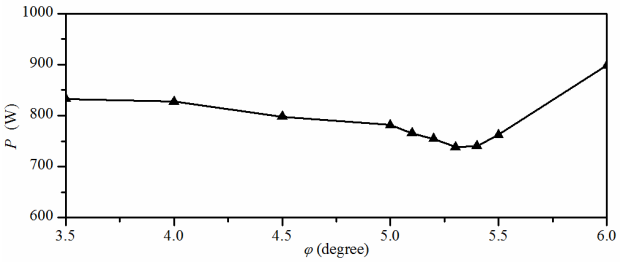

Figure 13. Total power loss versus the inner radius of sealing surface

IV. EXPERIMENT

A number of experimental investigations about slippers have been carried out. But the installation of sensors in the slipper/swash-plate pair is difficult due to the compact structure of the pump. Therefore, the test of slipper is out of the actual pump, resulting in the dynamic characteristics of the slipper deviating from the actual working conditions due to the structural simplification. In this paper the universal test platform of the pump is used to test the efficiency and working life of the pumps both with the original and the optimized slippers, validating the proposed optimization design method experimentally.

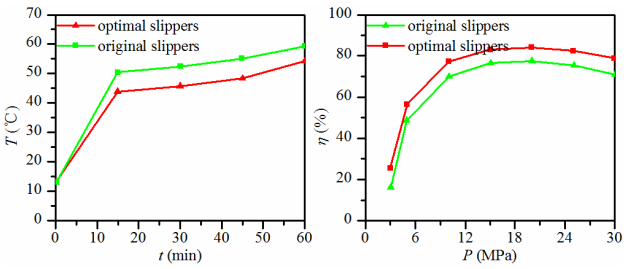

(a) Temperature (b) Efficiency

Figure 14. Comparison of optimized slippers and original slippers

Fig.14 shows the experimental results of optimized slippers and original slippers. The pump temperature and efficiency are measured at the same operating condition as the simulation parameters. The temperature of the pump with the original slippers is slightly higher than that of the pump with the optimized slippers, while the efficiency of the pump with the optimized slippers is slightly higher than that of the pump with the original slippers.

After the same period of working life test, the original pump broke down with a short working life due to slipper abrasion. The original inner radius of the slipper is 5.2mm. Fig.15 shows the wear condition of the slipper surface and the swash plate surface of the pump. It can be seen that partial abrasion of original slippers occur at the outside of the sealing surface due to the titling moments acted on slippers, and the wear trace at the outside edge is nearly uniform due to the slipper spin. The working condition becomes worse as the temperature increases. The retainer is destroyed and one of the slippers is taken off from the head of the piston. It can be concluded that the carrying ability of the oil film is insufficient, so solid-to-solid contact occurs between the slipper and the swash plate and the local internal force between the slipper and the swash plate is bigger than the pull-off force between the slipper and the piston. The wear of optimized slippers are mild, which means the lubrication condition between the slipper and the swash plate is rather good.

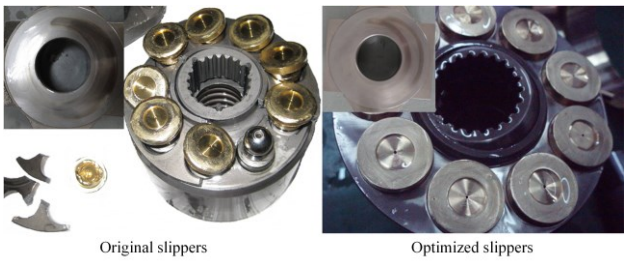

Figure 15. View of the tested slippers and swash plate

Above all, the optimized inner radius can improve the carrying ability of the oil film and reduce the power loss of the slipper/swash-plate pair apparently. The simulation model and optimization design method have a satisfying effect in the design of high-quality swash plate axial piston pump.

V. CONCLUSION

A dynamic lubrication model is developed in this paper taking oil film thickness, tilting angle and the slipper spin into consideration. The lubrication and wear mechanism are revealed by clarifying force conditions, oil film characteristics, hydrodynamic and squeezing effects in detail. The pressure peak and the bearing force center of the oil film for the tilted slipper locate at the side where the oil film thickness is small due to the hydrodynamic and squeezing effects. The slipper moves more steadily during the transition from low pressure to high pressure for the larger dynamic stiffness of the oil film. Then a reasonable design criterion is presented for the inner radius of sealing surface based on the optimum conditions, i.e. oil film characteristics, dynamic stiffness and minimum power loss. The simulation and experiment results both show that the optimized slipper has better lubrication condition, and the reliability and efficiency of the pump are improved. It verifies the design criterion has a high accuracy to great extent and it can be applied for the slipper optimization design for pump used in aerospace.

REFERENCES

[1] T. Kazama and A. Yamaguchi, " Optimum design of bearing and seal parts for hydraulic equipment," Wear, vol. 161, no. 1, pp: 161-171, 1993.

[2] X. Wang and A. Yamaguchi, "Characteristics of hydrostatic bearing/seal parts for water hydraulic pumps and motors. Part 1: Experiment and theory," Tribology international, vol. 35, no. 7, pp: 425-433,2002.

[3] X. Wang and A. Yamaguchi, "Characteristics of hydrostatic bearing/seal parts for water hydraulic pumps and motors. Part 2: On eccentric loading and power losses," Tribology international, vol. 35, no. 7, pp:435-442, 2002.

[4] N. Iboshi N and A. Yamaguchi, "Characteristics of a slipper bearing for swash plate type axial piston pumps and motors: 3rd Report, Design Method for a Slipper with a Minimum Power Loss in Fluid Lubrication," Bulletin of the JSME, vol. 29, no. 254, pp:2529-2538, 1986.

[5] C. J. Hooke and Y. P. Kakoullis, "The lubrication of slippers on axial piston pumps," presented at the 5th International Fluid Power Symposium, Durham, England, September, 1978, pp:13-26.

[6] C. J. Hooke and Y. P. Kakoullis, "The effects of centrifugal load and ball friction on the lubrication of slippers in axial piston pumps," presented at the 6th International Fluid Power Symposium, Cambridge, England, 1981, pp:179-191.

[7] C. J. Hooke and Y. P. Kakoullis, "The effects of non-flatness on the performance of slippers in axial piston pumps," Proceedings of the Institution of Mechanical Engineers, vol. 197(C), pp:239-247, 1983.

[8] C. J. Hooke and K. Y. Li, "The lubrication of overclamped slippers in axial piston pumps centrally loaded behavior," Proceedings of the Institution of Mechanical Engineers, vol.202(C4), pp:287-293, 1988.

[9] C.J. Hooke and K. Y. Li, "The lubrication of slippers in axial piston pumps and motors. The effect of tilting couples," Proceedings of the Institution of Mechanical Engineers, vol.203(C), pp:343-350, 1989.

[10] E. Koç, C. J. Hooke and K.Y. Li, "Slipper balance in axial piston pumps and motors," Transitions of the ASME, Journal of Tribology, vol.114, pp:766-772, 1992.

[11] E. Koç and C. J. Hooke, "Investigation into the effects of orifice size, offset and overclamp ratio on the lubrication of slipper bearings," Tribology International, vol. 29, no. 4, pp:299-305,1996.

[12] E. Koç and C. J. Hooke, "Considerations in the design of partially hydrostatic slipper bearings," Tribology International, vol. 20, no. 11, pp:815-823, 1997.

[13] F. Canbulut, "The experimental analyses of the effects of the geometric and working parameters on the circular hydrostatic thrust bearings," JSME International Journal Series C, vol. 48, no. 4, pp:715-722, 2005.

[14] R. M. Harris, K. A. Edge and D. G. Tilley, "Predicting the behavior of slipper pads in swashplate-type axial piston pumps," Journal of dynamic systems, measurement, and control, vol. 118, no.1 , pp:41-47, 1996.

[15] U. Wieczoreck U and M. Ivantysynova, "CASPAR-A computer aided design tool for axial piston machines," Proceedings of the power transmission motion and control international workshop, PTMC2000, Bath, UK. 2000, pp:113-126.

[16] U. Wieczorek U and M. Ivantysynova, "Computer aided optimization of bearing and sealing gaps in hydrostatic machines-the simulation tool CASPAR," International Journal of Fluid Power, vol. 3, no. 1, pp:7-20, 2002.

[17] C. C. Huang, "CASPAR based slipper performance prediction in axial piston pumps," Proceeding of the 3rd FPNI-PhD symposium on fluid power. Spain: E. Codina, 2004, PP:229-238.

[18] B. Zhang, B. Xu and C. L. Xia, "Modeling and simulation on axial piston pump based on virtual prototype technology," Chinese Journal of Mechanical Engineering, vol. 22, no. 1, 2009.

[19] B. Xu, J. H. Zhang and H. Y. Yang, "Investigation on the radial micro-motion about piston of axial piston pump," Chinese Journal of Mechanical Engineering, vol. 26, no. 2, pp:325-333, 2013.